

# Neural Point-Based Graphics

KARA-ALI ALIEV, Samsung AI Center

DMITRY ULYANOV, Samsung AI Center, Skolkovo Institute of Science and Technology

VICTOR LEMPITSKY, Samsung AI Center, Skolkovo Institute of Science and Technology

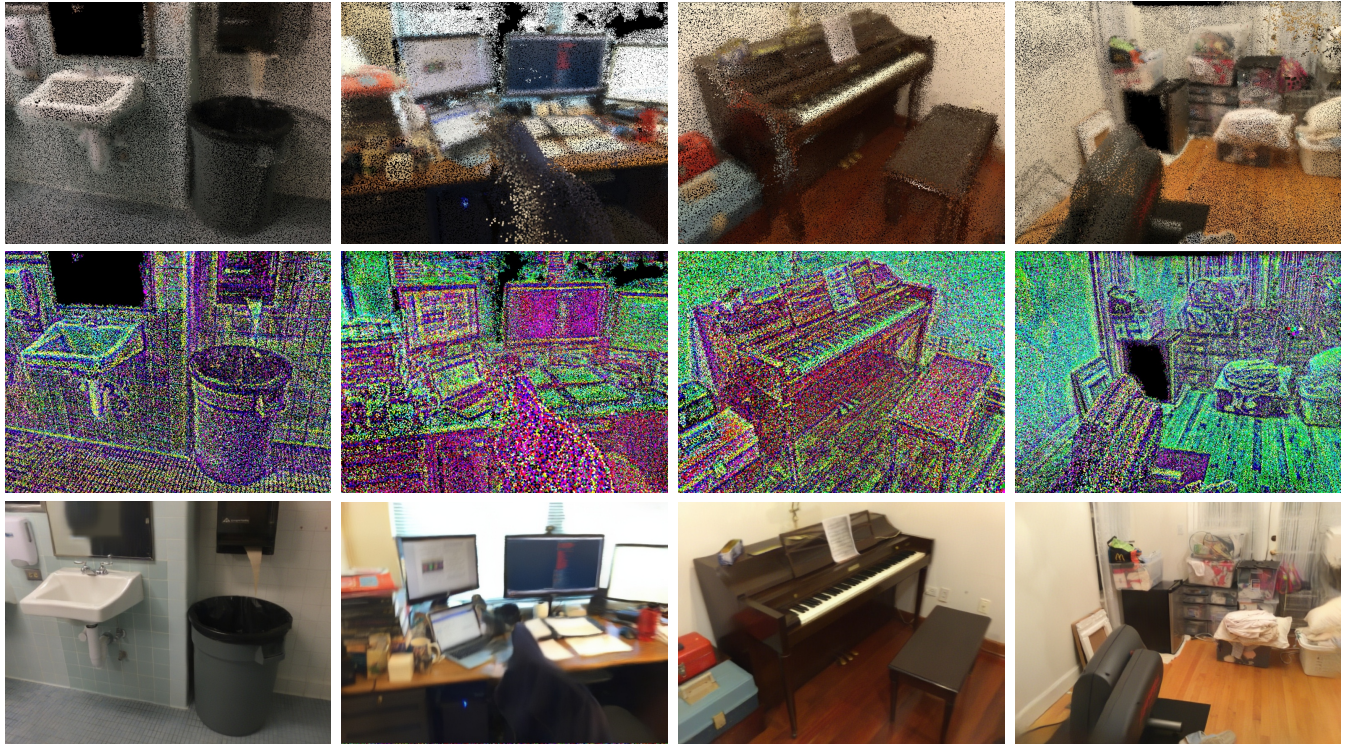


Fig. 1. Given a point cloud constructed from registered RGBD scans (top), our system learns the neural descriptors for every point (the first three PCA dimensions are shown in false color in the middle row), and a neural rendering network that maps the rasterized point descriptors to realistic images (bottom row). Gaps in geometry, geometric noise, and outlier points are inevitable in raw point clouds, such as these point clouds from the ScanNet dataset [7]. Our approach can handle these deficiencies gracefully and synthesizes realistic renderings despite them.

We present a new point-based approach for modeling complex scenes. The approach uses a raw point cloud as the geometric representation of a scene, and augments each point with a learnable neural descriptor that encodes local geometry and appearance. A deep rendering network is learned in parallel with the descriptors, so that new views of the scene can be obtained by passing the rasterizations of a point cloud from new viewpoints through this network. The input rasterizations use the learned descriptors as point pseudo-colors. We show that the proposed approach can be used for modeling complex scenes and obtaining their photorealistic views, while avoiding explicit surface estimation and meshing. In particular, compelling results are obtained for scene scanned using hand-held commodity RGB-D sensors

as well as standard RGB cameras even in the presence of objects that are challenging for standard mesh-based modeling.

Additional Key Words and Phrases: Point-based graphics, deep learning, 3D reconstruction, surfels, convolutional networks, BRDF estimation, normal estimation.

## 1 INTRODUCTION

Creating virtual models of real scenes usually involves a lengthy pipeline of operations. Such modeling usually starts with a scanning process, where the photometric properties are captured using camera images and the raw scene geometry is captured using depth scanners or dense stereo matching. The latter process usually provides noisy and incomplete point cloud that needs to be further processed by applying certain surface reconstruction and meshing approaches. Given the mesh, the texturing and material estimation

Authors' addresses: Kara-Ali Aliev, k.aliev@samsung.com, Samsung AI Center; Dmitry Ulyanov, d.ulianov@samsung.com, Samsung AI Center, Skolkovo Institute of Science and Technology; Victor Lempitsky, v.lempitsky@samsung.com, Samsung AI Center, Skolkovo Institute of Science and Technology.

processes determine the photometric properties of surface fragments and store them in the form of 2D parameterized maps, such as texture maps [4], bump maps [3], view-dependent textures [9], surface lightfields [48]. Finally, generating photorealistic views of the modeled scene involves computationally-heavy rendering process such as ray tracing and/or radiance transfer estimation.

The outlined pipeline has been developed and polished by the computer graphics researchers and practitioners for decades. Under controlled settings, this pipeline yields stunningly realistic results. Yet several of its stages (and, consequently, the entire pipeline) remain brittle, often require manual intervention of designers and photogrammetrists, and are challenged by certain classes of objects (e.g. thin objects).

Multiple streams of work aim to simplify the entire pipeline by eliminating some of its stages. Thus, image-based rendering techniques [16, 28, 33, 39] aim to obtain photorealistic views by warping the original camera images using certain (oftentimes very coarse) approximations of scene geometry. Alternatively, point-based graphics [17, 18, 26, 29] discards the estimation of the surface mesh and use a collection of points or unconnected disks (surfels) to model the geometry. More recently, deep rendering approaches [5, 6, 19, 21, 34] aim to replace physics-based rendering with a generative neural network, so that some of the mistakes of the modeling pipeline can be rectified by the rendering deep network.

Here, we present a system that eliminates most of the steps of the classical pipeline. It combines the ideas of image-based rendering, point-based graphics, and neural rendering into a simple approach. The approach uses the raw point-cloud as a scene geometry representation, thus eliminating the need for surface estimation and meshing. Similarly to other neural rendering approaches, it also uses a deep convolutional neural network to generate photorealistic renderings from new viewpoints. The realism of the rendering is facilitated by the estimation of latent vectors (neural descriptors) that describe both the geometric and the photometric properties of the data. The local descriptors are learned directly from data, and such learning happens in coordination with the learning of the rendering network (Figure 1).

We show that our approach is capable of modeling and rendering scenes that are captured by hand-held RGBD cameras as well as simple RGB streams (from which point clouds are reconstructed via stereo matching). A number of comparisons are performed with ablations and competing approaches, demonstrating the capabilities and advantages of the new method. In general, our results suggest that given the power of modern deep networks, the simplest 3D primitives (i.e. 3D points) represent sufficient and most suitable geometric proxies for neural rendering.

## 2 RELATED WORK

Our approach brings together several lines of works from computer graphics, computer vision, and deep learning communities.

### 2.1 Point-based graphics

Using points as the modeling primitives for rendering (point-based graphics) was proposed in [18, 29] and have been in active development in the 2000s [17, 26, 36, 51]. The best results are obtained

when each point is replaced with an oriented flat circular disk (a surfel), whereas the orientations and the radii of such disks can be estimated from the point cloud data. Multiple overlapping surfels are then rasterized and linearly combined using splatting operation [36]. Most recently, [5] has proposed to replace linear splatting with deep convolutional network. In our work, we follow the point-based graphics paradigm as we represent the geometry of a scene using its point cloud. However, we do not estimate the surface orientation, or suitable disk radii, or, in fact, even color, explicitly. Instead, we keep a 3D point as our modeling primitive and encode all local parameters of the surface (both photometric and geometric) within neural descriptors that are learned from data.

### 2.2 RGBD scene modeling

Since the introduction of Kinect, RGBD sensors have been actively used for scene modeling due to the combination of their low cost and their suitability for 3D geometry acquisition [8, 35]. Robust algorithms for RGBD-based simultaneous localization and mapping (SLAM) are now available [12, 24, 42, 47]. Most registration (SLAM) algorithms working with RGBD data construct dense volumetric scene representation, from which scene surface can be extracted e.g. using the marching cubes algorithm [31]. Such surface estimation procedure, however, is limited by the resolution of the underlying volumetric grid, and in general will lose e.g. thin details that might be present in the raw RGBD data. Our approach directly benefits from the availability of robust RGBD SLAM/registration algorithms, however it does not rely on the volumetric scene modeling and uses the point cloud assembled from the raw RGBD scans as the geometric model.

### 2.3 Surface lightfields

Since the inception of image-based rendering methods [33, 39], several ways to parameterize the plenoptic function [33] has been proposed. Among the most efficient is the *surface lightfields* [48]. This parameterization samples the plenoptic function densely at the surface of the scene. Namely, for a dense set of surface elements (parameterized using surface coordinates  $(u, v)$ ), the radiance/color along the rays along arbitrary 3D angles  $\alpha$  is recorded. Most recently, the deep variant of this parameterization was proposed in [6], where a fully-connected neural network accepting  $(u, v, \alpha)$  as an input is used to store the surface lightfield. The network parameters are learned from a dataset of images and a surface mesh. Our approach is related to approaches based on surface lightfields, as it implicitly learns the parameterization of pointwise plenoptic function at scene surface within the neural descriptors. Unlike surface lightfields, our approach does not require scene surface modeling. Also, differently from [6] that outputs color value independently in each surface vertex, we use a convolutional neural network for rendering, so that the output color value at a pixel depends on multiple neural descriptors and multiple points projected to the neighborhood of this pixel.

## 2.4 Image generation with ConvNets

Deep splatting [5] and deep surface lightfields [6] are examples of a fast growing body of work that use neural networks to generate photorealistic images [11]. Generally, these works benefit greatly from the work in machine learning and image processing on generative image modeling and deep image processing, and in particular on frameworks that use adversarial learning [15] and perceptual losses [10, 22] to train convolutional neural networks (ConvNets) [27] to output images (rather than to e.g. classify them).

Recent works have demonstrated the ability to synthesize high-resolution images [23] and to model sophisticated image [21, 46] and video [45] transformations using deep convolutional networks trained with such losses. In particular, [34] demonstrated how such *pixel-to-pixel* networks can be used to replace computationally-heavy rendering and to directly transform images with rasterized material properties and normal orientations to photorealistic views.

Also, highly relevant to our work are methods that successfully apply deep ConvNets for image inpainting tasks [20, 30, 49]. Several modifications to the convolutional architecture with the ability to handle and fill in holes have been suggested, and in our approach we use gated convolutional layers from [49].

## 2.5 Deep image based rendering

Recent years have also seen active convergence of image-based rendering and deep learning. A number of works combine warping of preexisting photographs and the use of neural networks to combine warped images and/or to post-process the warping result. The warping can be estimated by stereo matching [13]. Estimating warping fields from a single input image and a low-dimensional parameter specifying a certain motion from a low-parametric family is also possible [14, 50]. Other works perform warping using coarse mesh geometry, which can be obtained through multi-view stereo [19, 44] or volumetric RGBD fusion [32].

Alternatively, some methods avoid explicit warping and instead use some form of plenoptic function estimation and parameterization using neural networks. As mentioned above, [6] proposes network-parameterized deep version of surface lightfields. The approach [41] learns neural parameterization of the plenoptic function in the form of low-dimensional descriptors situated at the nodes of a regular voxel grid and a rendering function that turns the reprojection of such descriptors to the new view into an RGB image.

Most recent (and arguably most related to ours) is an independent parallel work [43]. They propose to learn *neural textures* encoding the point plenoptic function at different surface points alongside the neural rendering convolutional network. Our approach is similar to [43], as it also learns neural descriptors of surface elements jointly with the rendering network. The difference is that our approach uses point-based geometry representation and thus avoids the need for surface estimation and meshing.

## 3 METHODS

Below, we explain the details of our system. First, we explain how the rendering of a new view is performed given a point cloud with

learned neural descriptors and a learned rendering network. Afterwards, we discuss the learning process, as well as the adaptation of the learned system to new scenes.

### 3.1 Rendering

We first explain the rendering process. Assume that a point cloud  $\mathbf{P} = \{p_1, p_2, \dots, p_N\}$  with  $M$ -dimensional neural descriptors  $\mathbf{D} = \{d_1, d_2, \dots, d_N\}$  are given, and its rendering from a new view characterized by the camera  $C$  (including both extrinsic and intrinsic parameters) needs to be obtained. In particular, assume that the target image has  $W \times H$ -sized pixel grid, and that its viewpoint is located in point  $p_0$ .

The rendering is performed by first rasterizing each point  $p_i$  into a square with the side length that is inversely proportional to the depth of the point w.r.t. the camera  $C$ . The rendering is performed using OpenGL without anti-aliasing, so that the dimensions of each square are effectively rounded to the nearest integers. The Z-buffer algorithm is used for superimposing these squares onto each other using their depths w.r.t. the camera. Let  $f_i(C)$  denote the “footprint” set of the point  $s_i$  resulting from such rendering, i.e. a set of pixels that are occupied by the rasterization of the  $i$ -th square after z-buffer. We then create an  $(M + 3)$ -channel *raw image*  $S(\mathbf{P}, \mathbf{D}, C)$  by iterating over all footprint sets  $f_i(C)$  and filling all pixels from  $s_i(C)$  with the values of  $d_i$  (first  $M$  channels). The last three channels are set to the coordinates of the normalized viewpoint direction vector  $v_i = \frac{p_0 - p_i}{\|p_0 - p_i\|}$ . Thus, the pixels  $(x, y)$  of the raw image are filled as follows:

$$\forall (x, y) \in s_i : S(\mathbf{P}, \mathbf{D}, C)[x, y] = \{d_i; v_i\}, \quad (1)$$

where  $\{\}$  denotes concatenation, and  $[x, y]$  denotes the vectorial entry of the raw image corresponding to the pixel  $(x, y)$ . Concatenating the local surface information encoded within  $d_i$  with the viewpoint direction  $v_i$  allows our system to model view-dependent photometric effects, and also to fill-in the holes in the point-cloud network in a way that takes the relative orientation of the surface w.r.t. the viewpoint direction vector into account. The pixels not covered by any footprint are set to the special descriptor value  $d_0 \in R^M$  (which is also learned for a particular scene), and their viewpoint direction dimensions are set to zeros.

Finally, we use a pretrained *rendering network*  $\mathcal{R}_\theta$  with learnable parameters  $\theta$  to map the  $(M + 3)$ -channel raw image  $S(\mathbf{P}, \mathbf{D}, C)$  into a three-channel RGB image  $I$ :

$$I(\mathbf{P}, \mathbf{D}, C, \theta) = \mathcal{R}_\theta(S(\mathbf{P}, \mathbf{D}, C)). \quad (2)$$

The rendering network in our case has a popular convolutional U-Net architecture [37] with gated convolutions [49].

### 3.2 Learning

We now describe the learning process in our system. Learning is performed in a supervised way. We assume that during learning  $K$  training scenes are available. For the  $k$ -th scene the point cloud  $\mathbf{P}^k$  as well as the set of  $L_k$  training ground truth RGB images  $\mathbf{I}^k = \{I^{k,1}, I^{k,2}, \dots, I^{k,L_k}\}$  with known camera parameters  $\{C^{k,1}, C^{k,2}, \dots, C^{k,L_k}\}$  are given. Our learning objective  $\mathcal{L}$  then corresponds to the mismatch between the rendered and the ground

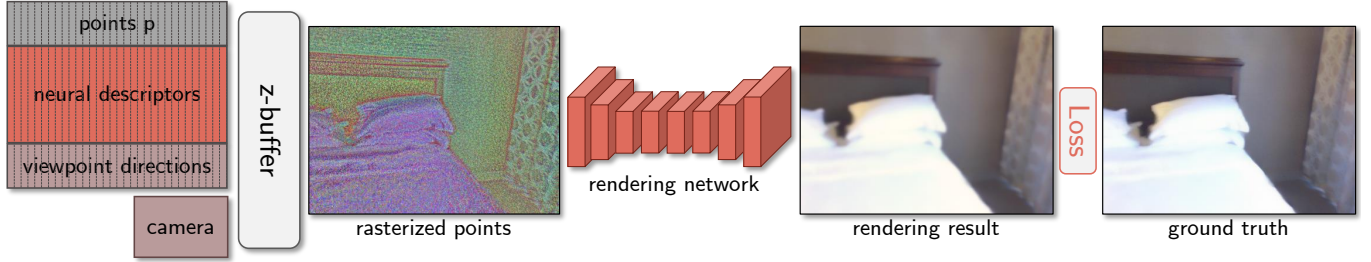


Fig. 2. An overview of our system. Given the point cloud  $P$  with neural descriptors  $D$  and camera parameters  $C$ , we estimate the viewpoint directions and then rasterize the points with z-buffer using the neural descriptors concatenated with viewpoint directions as pseudo-colors. Such rasterization is then passed through the rendering network to obtain the resulting image. Our model is fit to new scene(s) by optimizing the parameters of the rendering network and the neural descriptors by backpropagating the perceptual loss function.

truth RGB images:

$$\mathcal{L}(\theta, D^1, D^2, \dots, D^K) = \sum_{k=1}^K \sum_{l=1}^{L_k} \Delta \left( \mathcal{R}_\theta \left( S(P^k, D^k, C^{k,l}) \right), I^{k,l} \right), \quad (3)$$

where  $D^k$  denotes the set of neural descriptors for the point cloud of the  $k$ -th scene, and  $\Delta$  denotes the mismatch between the two images (the ground truth and the rendered one). In our implementation, we use the perceptual loss [10, 22] that computes the mismatch between the activations of a pretrained VGG network [40].

The learning is performed by optimizing the loss (3) over both the parameters  $\theta$  of the rendering network **and** the neural descriptors  $\{D^1, D^2, \dots, D^K\}$  of points in the training set of scenes. Thus, our approach learns the neural descriptors directly from data. Optimization is performed by the ADAM algorithm [25]. Note, that the neural descriptors are updated via backpropagation through (1) of the loss derivatives w.r.t.  $S(P, D, C)$  onto  $d_i$ .

### 3.3 Modeling new scenes

After the learning (3) is performed, a new scene can be modeled by our system given its point cloud and a set of RGB views registered with this point cloud. For example, in the case of the scene scanned with an RGBD camera, the registered RGBD views can provide both the point cloud and the RGB views.

For a new scene, given a point cloud  $P'$  and a set of images  $I' = \{I'^1, I'^2, \dots, I'^{L'}\}$  with camera parameters  $\{C'^1, C'^2, \dots, C'^{L'}\}$ , we learn the neural descriptors  $D' = \{d'_1, d'_2, \dots, d'_{N'}\}$  of the new scene, while keeping the parameters  $\theta$  fixed, by optimizing the objective  $\mathcal{L}'$ :

$$\mathcal{L}'(D') = \sum_{l=1}^{L'} \Delta \left( \mathcal{R}_\theta \left( S(P', D', C'^l) \right), I'^l \right). \quad (4)$$

By sharing the rendering parameters  $\theta$  between the training scene and the new scene, our system is capable of better generalization resulting in a better new view synthesis.

Alternatively, rather than keeping the parameters  $\theta$  of the rendering network fixed, we can fine-tune them to the new scene, using the pre-learned values as initializations. For some scenes, we observe modest improvements in the rendering quality of new views from

such fine-tuning. In practical systems, however, it may be desirable to keep the rendering network compatible across multiple scenes (i.e. to have a *universal* rendering network).

### 3.4 Experimental details

Our model is based on a popular U-Net [38] architecture with four downsampling and upsampling blocks. We substituted max pooling layers with average pooling layers and transposed convolutions with bilinear upsampling layers. We observed that gated convolutions [49] improve performance of the model on sparse input data, so normal convolutions are substituted with gated convolutions in our model. Since we use U-Net as our rendering network and learn rich point features separately, it turns out we can use lightweight network with fewer parameters. Our model has four times fewer channels in each convolutional layer than in the original architecture, resulting in 1.96M parameters. It allows us to render real-time, taking TODOMs on GeForce RTX 2080 Ti to render a 1296x968 image.

## 4 EXPERIMENTS

### 4.1 Datasets

To demonstrate the versatility of the approach, we evaluate it on several types of scenes. We are primarily interested in the capture of real scenes using consumer low-cost devices. Thus, we consider two types of capture. First, we consider RGBD streams from the ScanNet dataset [7] of room-scale scenes scanned with a structured-light RGBD sensor<sup>1</sup>. Second, we consider the RGB video streams captured by a smartphone. Finally, we demonstrate the relevance of our approach to modeling of photometrically-complex synthetic scenes by running it on a standard test scene from the Blender software [2].

For the ScanNet scenes, we use the provided registration data obtained with the BundleFusion [8] dataset. We also use the mesh geometry computed by BundleFusion in the respective baselines. Given the registration data, point clouds are obtained by joining together the 3D points from all RGBD frames and using volumetric subsampling (with the grid step 1 cm) resulting in the point clouds containing few million points per scene.

<sup>1</sup><https://structure.io/>

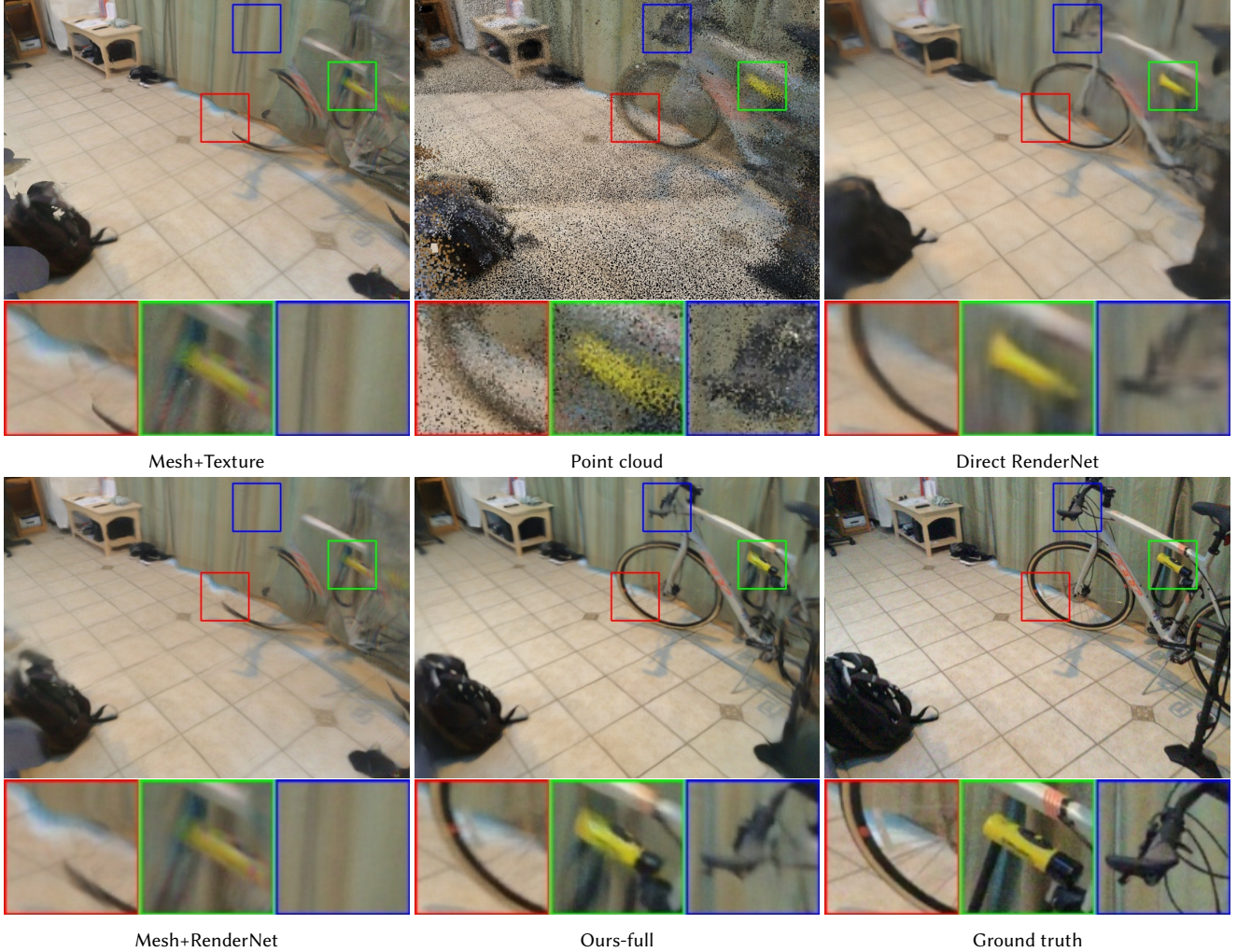


Fig. 3. Comparative results on the 'Studio' dataset (from [7]). We show the textured mesh, the colored point cloud, the results of three neural rendering systems (including ours), and the ground truth. Our system can successfully reproduce details that pose challenging for meshing, and suffers less from blurriness than the Direct RenderNet system.

In the evaluation, we use two ScanNet scenes '**Studio**' (scene 0), which has 5578 frames, and '**LivingRoom**' (scene 24), which has 3300 frames. In each case, we use every 100th frames in the trajectory for validation. We then removed frames within 20 time steps from each of these validation frames from the fitting set, using remaining 3303 and 2007 frames respectively for the fitting (fine-tuning) and descriptor estimation. We pretrain rendering networks on the set of 52 scenes (preprocessed in a similar fashion) that does not include Studio and LivingRoom scenes.

For the smartphone-captured scenes, we have run the commercial Agisoft Metashape [1] package, which is one of the best packages for scene modeling/reconstruction. Agisoft Metashape provides the registration, the point cloud, and the mesh by running proprietary structure-and-motion and dense multiview stereo methods. We evaluate on two scenes: '**Shoe**' and '**Plant**'. The plant scene contains

2727 frames taken with 250ms intervals, out of which we put every 50th into the validation set and withhold 10 frames around these frames and use the rest as the fitting set. The *shoe* scene has been taken deliberately very small number of images, as it contains 100 frames taken with 250ms intervals, which we shuffle and hold out 10 frames for validation.

## 4.2 Compared approaches

We compare several approaches on the evaluation scenes. Most of these approaches have a rendering network similar to our method, which takes an intermediate representation and then is trained to output the final RGB image. Unless stated otherwise, we use the network described in Section 3.4 (with 1.96M parameters) for all methods.

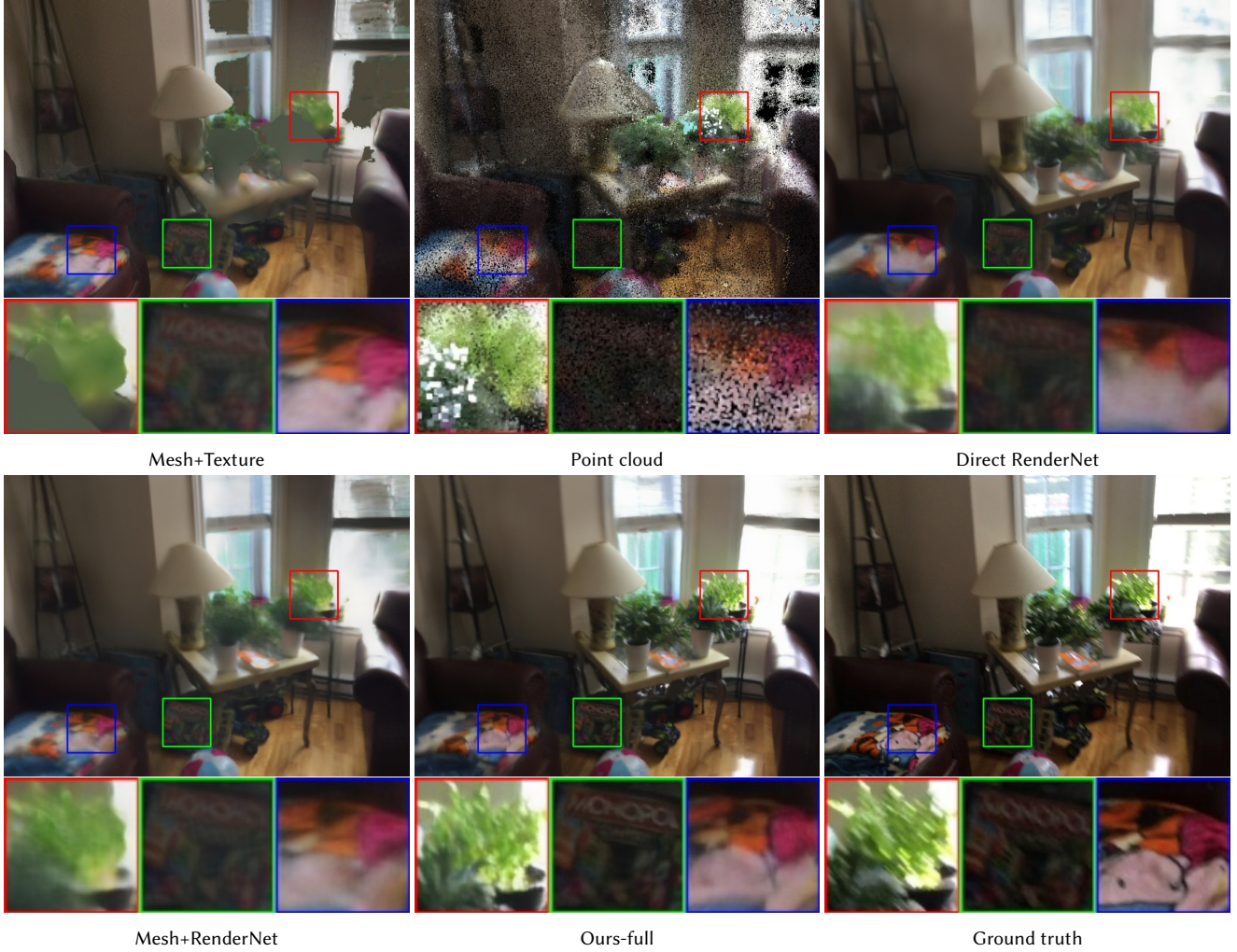


Fig. 4. Comparative results on the 'LivingRoom' dataset (from [7]) – same format as in Figure 3.

Method	Studio (RGBD stream) Loss $\downarrow$ PSNR $\uparrow$ SSIM $\uparrow$	LivingRoom (RGBD stream) Loss $\downarrow$ PSNR $\uparrow$ SSIM $\uparrow$	Shoe (RGB video) Loss $\downarrow$ PSNR $\uparrow$ SSIM $\uparrow$	Plant (RGB video) Loss $\downarrow$ PSNR $\uparrow$ SSIM $\uparrow$	RenderNet params
Mesh+texture	551.193 18.372 0.821	678.957 15.373 0.764	378.502 20.229 0.852	482.707 18.822 0.746	-
Mesh+RenderNet	539.210 19.180 0.840	581.367 17.536 0.819	<b>280.242 24.062 0.910</b>	375.322 21.846 <b>0.817</b>	1.96M
Ours-scene	<b>523.287 19.615 0.841</b>	<b>545.406 18.486 0.828</b>	284.617 23.851 0.888	<b>340.275 22.674 0.817</b>	1.96 M
*Direct RenderNet	528.705 18.185 0.819	557.513 16.840 0.793	265.722 22.552 0.890	363.445 21.888 0.801	1.96 M
*Direct RenderNet (slow)	518.310 19.814 0.850	534.648 18.834 0.840	<b>260.530 25.936 0.920</b>	345.232 23.334 0.837	7.84 M
*Ours-full	<b>508.182 19.899 0.852</b>	<b>525.016 18.888 0.842</b>	260.981 25.330 0.917	<b>323.483 23.655 0.844</b>	1.96 M
*Ours-universal	510.135 <b>19.900 0.863</b>	525.043 <b>18.894 0.842</b>	<b>259.528 25.524 0.917</b>	<b>323.483 23.655 0.844</b>	1.96 M

Table 1. Comparison results in terms of the perceptual loss (lower is better), PSNR (higher is better), SSIM (higher is better) measures. The methods marked with \* have been pretrained on a hold-out scene dataset. See text for the description of methods. In general, the variants of our method outperforms the baselines and TODO.



Fig. 5. Comparative results on the 'Plant' dataset – same format as in Figure 3.

- **Ours-adapted.** This is a variant of our system, where the rendering network and the descriptor space are pretrained on the 52 ScanNet scenes. Then we learn the neural descriptors and fine-tune (adapt) the rendering network on the fitting part of the evaluation scene. Such fine-tuning converges after 30 epochs (8 minutes to 1.5 hours on 4x NVIDIA Tesla V-100 depending on the size of the scene).
- **Ours-universal.** In this variant, we do the same as above. However the rendering network is not fine-tuned for the evaluation scheme and is kept fixed, while the neural descriptors of the points are trained. Keeping the rendering network “universal”, i.e. unadapted to a specific scene may be more practical in many scenarios. Such learning converges after 20 epochs (5 minutes to 1 hour on 4x NVIDIA Tesla V-100 depending on the size of the scene).
- **Ours-Scene.** In this variant, we do not pretrain the rendering network, and instead learn it on the evaluation scene (its

fitting part) only, alongside the point descriptors. Naturally, such approach is more prone to overfitting. Such learning converges after 50 epochs (12 minutes to 2.5 hours on 4x NVIDIA Tesla V-100 depending on the size of the scene).

- **Mesh+Texture.** In this baseline, given the mesh of the scene obtained with BundleFusion or Metashape, we learn the texture via backpropagation of the same loss as used in our method through the texture mapping process onto the texture map. This results in a “classical” scene representation of the textured mesh.
- **Mesh+RenderNet.** In this variant (similar to e.g. Lookin-Good [32]), we additionally learn the rendering network that maps the rasterizations of the textured mesh into the final RGB images. The rendering network has the same architecture as ours (except that the input has three channels), and the learning uses the same loss as ours.

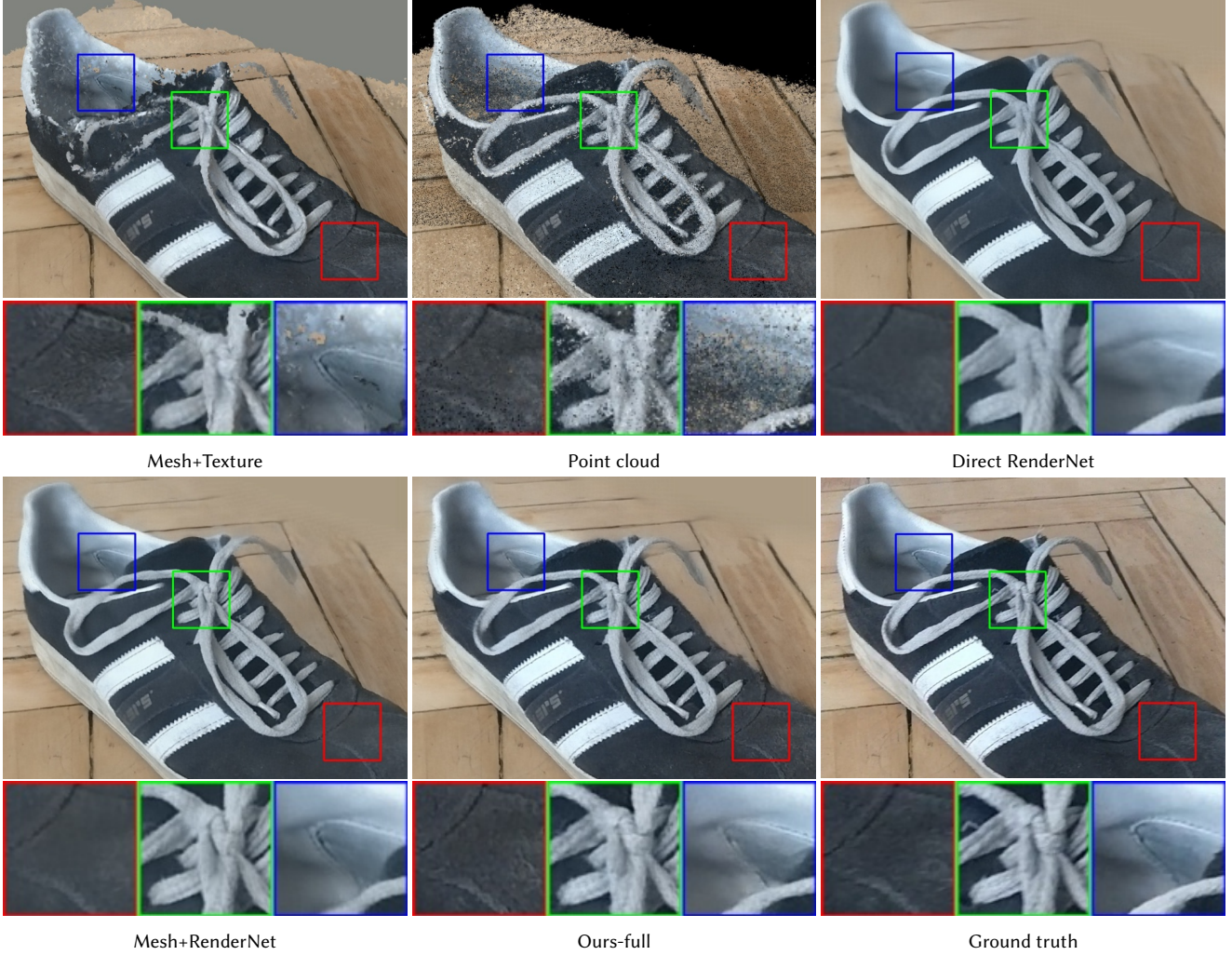


Fig. 6. Comparative results on the 'Shoe' dataset – same format as in Figure 3. Unlike the other three datasets, the geometry of this scene was more suitable for mesh representation, and the mesh-based rendering performs relatively well. Our method again outperforms the Direct RenderNet baseline.

- **Direct RenderNet.** In this variant, we evaluate an ablation of our point-based system without neural descriptors. Here, we learn the rendering network that maps the point cloud rasterized in the same way as in our method. However, instead of neural descriptors, we use the color of the point (taken from the original RGBD scan/RGB image), the 3D coordinate of the point, and the viewpoint direction  $v_i$  as a 9D pseudocolor. The rendering network is then trained with the same loss as ours. The rendering network is also pretrained on the set of 52 scenes.
- **Direct RenderNet (slow).** We observed that the Direct RenderNet variant described above benefits considerably from higher-capacity and slower rendering network. We therefore evaluated the variant with the rendering network with doubled number of channels in all intermediate layers (resulting in 4x params, 4x FLOPs).

We have also invested a significant effort into adapting the surface lightfields approach [6] to our data. We, however, seldom observe any improvement over the Mesh+Texture variant, and on average the results on hold-out data was worse. Apparently, surface light field estimation is not suitable for the cases when the mesh geometry is coarse.

### 4.3 Comparison results

The quantitative results of the comparison are shown in Table 1. All comparisons are measured on the validation subsets, for which we compare the obtained and the ground truth RGB images. We report the value of the loss on these subsets (note that this comparison is valid, since most of the methods optimize the same loss on the training set). We also report the the peak signal-to-noise ration (PSNR) and the self-similarity measure (SSIM). We also show qualitative

comparisons on the validation set frames in Figures 3-6, where we also show the point cloud.

Generally, both the quantitative and the qualitative comparison reveals the advantage of **using the point cloud as the geometric proxy**. Thus, Mesh+texture and Mesh+RenderNet perform worse than all methods that use the point clouds. The exception is the Shoe scene, where the meshing procedure was successful at generating a reasonably good mesh. In all other scenes, there are parts of the scene where the meshing process (BundleFusion or Metashape) has failed, leading to gross mistakes in the renderings. The qualitative comparison reveals such failures that are particularly notorious on thin objects (such as the details of the bicycle in Figure 3 or the leaves of the plant in Figure 5).

We also observe that our system based on neural descriptors of the point generally outperforms the direct RenderNet ablation, which does not have such descriptors. We also note, that our validation frames are not too far from the fitting set, and we observe that qualitatively the difference between methods becomes larger when camera is moved further from the fitting set cameras. The effect of this can be observed in **supplementary video**. Generally, the quality of single frames for such camera positions is considerably better for our method than for the Direct baseline (which suffers from blurriness and loss of details). At the same time, admittedly, this strong improvement in the quality of individual frames comes at the price of increased temporal flickering.

#### 4.4 Results on synthetic data

We also show the capability of our approach to model synthetic scenes with extremely complex photometric properties (Figure 7). Here, the use of our approach may be justified as a means for accelerating rendering. Towards this end, we take the default Blender [2] test scene with complex lighting and highly-specular object in the center, sample a point cloud (2.5 million points) from its surface, and learn the neural descriptors and the rendering networks from 200 random views of the scene. The comparison of our renderings with the “ground truth” synthetic renderings obtained by ray tracing within Blender reveals very close match (Figure 7). While Blender takes about 2 minutes to render one frame of this scene on two GeForce RTX 2080 Ti (highest quality setting), our renderings are obtained at 50ms (20 frames-per-second) on one GeForce RTX 2080 Ti. We note that given the availability of a good surface mesh for this scene, mesh-based neural rendering approaches [6, 19, 43] are also likely to perform well at this task.

## 5 DISCUSSION

We have presented a neural point-based approach for modeling complex scenes. Similarly to classical point-based approaches, ours uses 3D points as modeling primitives. Each of the points in our approach is associated with a local descriptor containing information about local geometry and appearance. A rendering network that translates point rasterizations into realistic views, while taking the learned descriptors as an input point pseudo-colors, is learned in parallel with the descriptors themselves.

The learning process is performed using a dataset of point clouds and images. After learning, our model can be fitted to new scenes

and is capable of producing realistic views from new viewpoints. Notably, our system accomplishes this in a purely data-driven manner, while avoiding meshing, or any other form of explicit surface reconstruction, as well as without performing explicit geometric and photometric surface parameter estimation.

Our main contribution is the demonstration that point clouds can be successfully used as geometric proxies for neural rendering, while missing information about connectivity as well as geometric noise and holes can be handled by deep rendering networks gracefully. We have also shown that the model benefits from pretraining on a corpus of scenes, and that good results can be obtained with a universal rendering network that has not been fine-tuned for a particular scene.

**Limitations and improvements.** Our model currently cannot fill very big holes in geometry in a realistic way. Such ability is likely to come with additional point cloud processing/inpainting that could potentially be trained jointly with our modeling pipeline. We have also not investigated the performance of the system for dynamic scenes, where some update mechanism for the neural descriptors of points would need to be introduced.

## 6 ACKNOWLEDGEMENTS

The authors acknowledge the usage of the Skoltech CDISE HPC cluster ZHORES for obtaining the results presented in this paper.

## REFERENCES

- [1] Agisoft. retrieved 20.05.2019. *Metashape software*. <https://www.agisoft.com/>
- [2] Blender Online Community. retrieved 20.05.2019. *Blender - a 3D modelling and rendering package*. Blender Foundation, Blender Institute, Amsterdam. <http://www.blender.org>
- [3] James F Blinn. 1978. Simulation of wrinkled surfaces. In *Proc. SIGGRAPH*, Vol. 12. ACM, 286–292.
- [4] James F Blinn and Martin E Newell. 1976. Texture and reflection in computer generated images. *Commun. ACM* 19, 10 (1976), 542–547.
- [5] Giang Bui, Truc Le, Brittany Morago, and Ye Duan. 2018. Point-based rendering enhancement via deep learning. *The Visual Computer* 34, 6–8 (2018), 829–841.
- [6] Anpei Chen, Minye Wu, Yingliang Zhang, Nianyi Li, Jie Lu, Shenghua Gao, and Jingyi Yu. 2018. Deep Surface Light Fields. *Proceedings of the ACM on Computer Graphics and Interactive Techniques* 1, 1 (2018), 14.
- [7] Angela Dai, Angel X. Chang, Manolis Savva, Maciej Halber, Thomas Funkhouser, and Matthias Nießner. 2017. ScanNet: Richly-annotated 3D Reconstructions of Indoor Scenes. In *Proc. CVPR*.
- [8] Angela Dai, Matthias Nießner, Michael Zollhöfer, Shahram Izadi, and Christian Theobalt. 2017. BundleFusion: Real-Time Globally Consistent 3D Reconstruction Using On-the-Fly Surface Reintegration. *ACM Trans. Graph.* 36, 3 (2017), 24:1–24:18.
- [9] Paul Debevec, Yizhou Yu, and George Borshukov. 1998. Efficient view-dependent image-based rendering with projective texture-mapping. In *Rendering Techniques*. Springer, 105–116.
- [10] Alexey Dosovitskiy and Thomas Brox. 2016. Generating Images with Perceptual Similarity Metrics based on Deep Networks. In *Proc. NIPS*, 658–666.
- [11] Alexey Dosovitskiy, Jost Tobias Springenberg, and Thomas Brox. 2015. Learning to generate chairs with convolutional neural networks. In *Proc. CVPR*. 1538–1546.
- [12] Felix Endres, Jürgen Hess, Jürgen Sturm, Daniel Cremers, and Wolfram Burgard. 2014. 3-D mapping with an RGB-D camera. *IEEE transactions on robotics* 30, 1 (2014), 177–187.
- [13] John Flynn, Ivan Neulander, James Philbin, and Noah Snavely. 2016. Deepstereo: Learning to predict new views from the world’s imagery. In *Proceedings of the IEEE Conference on Computer Vision and Pattern Recognition*. 5515–5524.
- [14] Yaroslav Ganin, Daniil Kononenko, Diana Sungatullina, and Victor S. Lempitsky. 2016. DeepWarp: Photorealistic Image Resynthesis for Gaze Manipulation. In *Proc. ECCV*. 311–326.
- [15] Ian Goodfellow, Jean Pouget-Abadie, Mehdi Mirza, Bing Xu, David Warde-Farley, Sherjil Ozair, Aaron Courville, and Yoshua Bengio. 2014. Generative adversarial nets. In *Proc. NIPS*. 2672–2680.
- [16] Steven J. Gortler, Radek Grzeszczuk, Richard Szeliski, and Michael F. Cohen. 1996. The Lumigraph. In *SIGGRAPH ACM*, 43–54.

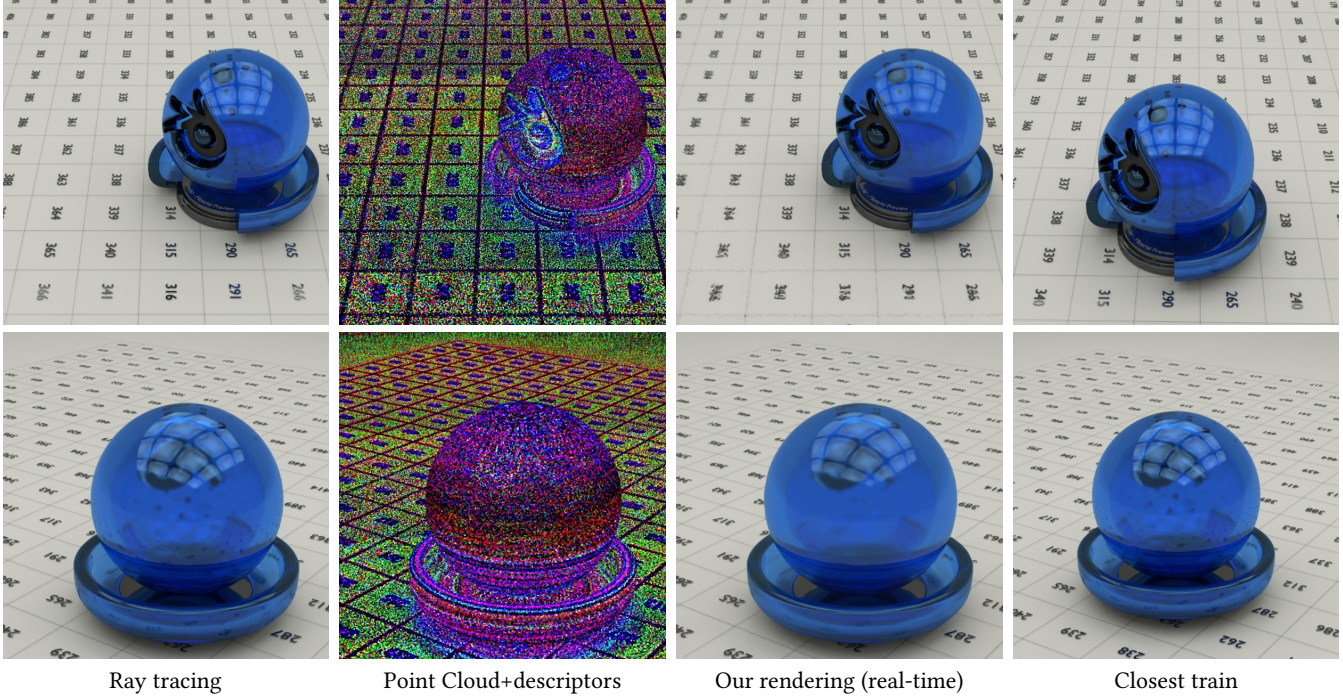


Fig. 7. Our system can be used to speed up renderings of synthetic scenes. Here, we show renderings of the standard Blender test scene using our system (third column). The closest frame from the dataset of frames used for model fitting is shown the fourth column. While our system does not match the result of the ray tracing rendering exactly, it manages to reproduce some details in the specular reflection, and fine details in the texture, while doing so at real-time speed.

- [17] Markus Gross, Hanspeter Pfister, Marc Alexa, Mark Pauly, Marc Stamminger, and Matthias Zwicker. 2002. *Point based computer graphics*. Eurographics Assoc.
- [18] Jeffrey P Grossman and William J Daly. 1998. Point sample rendering. In *Rendering Techniques'98*. Springer, 181–192.
- [19] Peter Hedman, Julien Philip, True Price, Jan-Michael Frahm, George Drettakis, and Gabriel J. Brostow. 2018. Deep blending for free-viewpoint image-based rendering. *ACM Trans. Graph.* 37, 6 (2018), 257:1–257:15.
- [20] Satoshi Iizuka, Edgar Simo-Serra, and Hiroshi Ishikawa. 2017. Globally and Locally Consistent Image Completion. *ACM Transactions on Graphics (Proc. of SIGGRAPH 2017)* 36, 4, Article 107 (2017), 107:1–107:14 pages.
- [21] Phillip Isola, Jun-Yan Zhu, Tinghui Zhou, and Alexei A. Efros. 2017. Image-to-Image Translation with Conditional Adversarial Networks. In *Proc. CVPR*. 5967–5976.
- [22] Justin Johnson, Alexandre Alahi, and Li Fei-Fei. 2016. Perceptual Losses for Real-Time Style Transfer and Super-Resolution. In *Proc. ECCV*. 694–711.
- [23] Tero Karras, Timo Aila, Samuli Laine, and Jaakko Lehtinen. 2018. Progressive Growing of GANs for Improved Quality, Stability, and Variation. In *International Conference on Learning Representations*. <https://openreview.net/forum?id=Hk992CeAb>
- [24] Christian Kerl, Jürgen Sturm, and Daniel Cremers. 2013. Dense visual SLAM for RGB-D cameras. In *Proc. IROS*. IEEE, 2100–2106.
- [25] Diederik P. Kingma and Jimmy Ba. 2014. Adam: A Method for Stochastic Optimization. *CoRR* abs/1412.6980 (2014). arXiv:1412.6980
- [26] Leif Kobbelt and Mario Botsch. 2004. A survey of point-based techniques in computer graphics. *Computers & Graphics* 28, 6 (2004), 801–814.
- [27] Yann LeCun, Bernhard Boser, John S Denker, Donnie Henderson, Richard E Howard, Wayne Hubbard, and Lawrence D Jackel. 1989. Backpropagation applied to handwritten zip code recognition. *Neural computation* 1, 4 (1989), 541–551.
- [28] Marc Levoy and Pat Hanrahan. 1996. Light field rendering. In *Proceedings of the 23rd annual conference on Computer graphics and interactive techniques*. ACM, 31–42.
- [29] Marc Levoy and Turner Whitted. 1985. *The use of points as a display primitive*. Citeseer.
- [30] Guilin Liu, Fitzsum A Reda, Kevin J Shih, Ting-Chun Wang, Andrew Tao, and Bryan Catanzaro. 2018. Image inpainting for irregular holes using partial convolutions. In *Proceedings of the European Conference on Computer Vision (ECCV)*. 85–100.
- [31] William E Lorensen and Harvey E Cline. 1987. Marching cubes: A high resolution 3D surface construction algorithm. In *Proc. SIGGRAPH*, Vol. 21. 163–169.
- [32] Ricardo Martin-Brualla, Rohit Pandey, Shuoran Yang, Pavel Pidlypenskiy, Jonathan Taylor, Julien Valentin, Sameh Khamis, Philip Davidson, Anastasia Tkach, Peter Lincoln, et al. 2018. LookinGood: enhancing performance capture with real-time neural re-rendering. In *SIGGRAPH Asia 2018 Technical Papers*. ACM, 255.
- [33] Leonard McMillan and Gary Bishop. 1995. Plenoptic modeling: an image-based rendering system. In *SIGGRAPH*. ACM, 39–46.
- [34] Oliver Nalbach, Elena Arabadzhyska, Dushyant Mehta, Hans-Peter Seidel, and Tobias Ritschel. 2017. Deep Shading: Convolutional Neural Networks for Screen Space Shading. *Comput. Graph. Forum* 36, 4 (2017), 65–78.
- [35] Richard A. Newcombe, Shahram Izadi, Otnar Hilliges, David Molyneaux, David Kim, Andrew J. Davison, Pushmeet Kohli, Jamie Shotton, Steve Hodges, and Andrew W. Fitzgibbon. 2011. KinectFusion: Real-time dense surface mapping and tracking. In *ISMAR*. IEEE Computer Society, 127–136.
- [36] Hanspeter Pfister, Matthias Zwicker, Jeroen Van Baar, and Markus Gross. 2000. Surfels: Surface elements as rendering primitives. In *Proceedings of the 27th annual conference on Computer graphics and interactive techniques*. ACM Press/Addison-Wesley Publishing Co., 335–342.
- [37] Olaf Ronneberger, Philipp Fischer, and Thomas Brox. 2015. U-net: Convolutional networks for biomedical image segmentation. In *International Conference on Medical image computing and computer-assisted intervention*. Springer, 234–241.
- [38] Olaf Ronneberger, Philipp Fischer, and Thomas Brox. 2015. U-Net: Convolutional Networks for Biomedical Image Segmentation. *CoRR* abs/1505.04597 (2015). arXiv:1505.04597 <http://arxiv.org/abs/1505.04597>
- [39] Steven M Seitz and Charles R Dyer. 1996. View morphing. In *Proceedings of the 23rd annual conference on Computer graphics and interactive techniques*. ACM, 21–30.
- [40] Karen Simonyan and Andrew Zisserman. 2014. Very Deep Convolutional Networks for Large-Scale Image Recognition. *CoRR* abs/1409.1556 (2014). arXiv:1409.1556 <http://arxiv.org/abs/1409.1556>
- [41] Vincent Sitzmann, Justus Thies, Felix Heide, Matthias Nießner, Gordon Wetzstein, and Michael Zollhöfer. 2019. DeepVoxels: Learning Persistent 3D Feature Embeddings. In *Proc. CVPR*.

[42] Jürgen Sturm, Nikolas Engelhard, Felix Endres, Wolfram Burgard, and Daniel Cremers. 2012. A benchmark for the evaluation of RGB-D SLAM systems. In *Proc. IROS*. IEEE, 573–580.

[43] Justus Thies, Michael Zollhöfer, and Matthias Nießner. 2019. Deferred Neural Rendering: Image Synthesis using Neural Textures. In *Proc. SIGGRAPH*.

[44] J. Thies, M. Zollhöfer, C. Theobalt, M. Stamminger, and M. Nießner. 2018. IGNOR: Image-guided Neural Object Rendering. *arXiv 2018* (2018).

[45] Ting-Chun Wang, Ming-Yu Liu, Jun-Yan Zhu, Guilin Liu, Andrew Tao, Jan Kautz, and Bryan Catanzaro. 2018. Video-to-Video Synthesis. In *Proc. NIPS*.

[46] Ting-Chun Wang, Ming-Yu Liu, Jun-Yan Zhu, Andrew Tao, Jan Kautz, and Bryan Catanzaro. 2018. High-Resolution Image Synthesis and Semantic Manipulation with Conditional GANs. In *Proc. CVPR*.

[47] Thomas Whelan, Michael Kaess, Hordur Johannsson, Maurice Fallon, John J Leonard, and John McDonald. 2015. Real-time large-scale dense RGB-D SLAM with volumetric fusion. *The International Journal of Robotics Research* 34, 4-5 (2015), 598–626.

[48] Daniel N Wood, Daniel I Azuma, Ken Aldinger, Brian Curless, Tom Duchamp, David H Salesin, and Werner Stuetzle. 2000. Surface light fields for 3D photography. In *Proc. SIGGRAPH*. 287–296.

[49] Jiahui Yu, Zhe Lin, Jimei Yang, Xiaohui Shen, Xin Lu, and Thomas S Huang. 2018. Free-Form Image Inpainting with Gated Convolution. *arXiv preprint arXiv:1806.03589* (2018).

[50] Tinghui Zhou, Shubham Tulsiani, Weilun Sun, Jitendra Malik, and Alexei A Efros. 2016. View synthesis by appearance flow. In *Proc. ECCV*. 286–301.

[51] Matthias Zwicker, Hanspeter Pfister, Jeroen Van Baar, and Markus Gross. 2001. Surface splatting. In *Proc. SIGGRAPH*. ACM, 371–378.